THE JOURNAL OF BIOLOGICAL CHEMISTRY VOL. 289, NO. 17, pp. 12063–12076, April 25, 2014

The Lantibiotic NAI-107 Binds to Bactoprenol-bound Cell Wall Precursors and Impairs Membrane Functions*[S]

Received for publication, November 22, 2013, and in revised form, February 19, 2014 Published, JBC Papers in Press, March 13, 2014, DOI 10.1074/jbc.M113.537449

Daniela Münch[‡1], Anna Müller[‡], Tanja Schneider[‡], Bastian Kohl[§], Michaela Wenzel[§], Julia Elisabeth Bandow[§2], Sonia Maffioli[¶], Margherita Sosio[¶], Stefano Donadio[¶], Reinhard Wimmer[‖], and Hans-Georg Sahl[‡3]

From the [‡]Institute of Medical Microbiology, Immunology and Parasitology, Pharmaceutical Microbiology Section, University of Bonn, 53115 Bonn, Germany, the [§]Department of Biology of Microorganisms, Ruhr University Bochum, 44780 Bochum, Germany, the [¶]NAICONS, Srl, 20139 Milano, Italy, and the [‖]Department of Biotechnology, Chemistry and Environmental Engineering, Aalborg University, 9000 Aalborg, Denmark

Background: NAI-107 is a potent lantibiotic with an unknown mode of action.
Results: NAI-107 targets bactoprenol-bound cell envelope precursors, *e.g.* lipid II, and in addition affects the bacterial membrane.
Conclusion: Cell wall biosynthesis is blocked by sequestration of lipid II and functional disorganization of the cell wall machinery.
Significance: The dual mechanism of action may explain the potency of NAI-107 and related lantibiotics.

The lantibiotic NAI-107 is active against Gram-positive bacteria including vancomycin-resistant enterococci and methicillin-resistant *Staphylococcus aureus*. To identify the molecular basis of its potency, we studied the mode of action in a series of whole cell and *in vitro* assays and analyzed structural features by nuclear magnetic resonance (NMR). The lantibiotic efficiently interfered with late stages of cell wall biosynthesis and induced accumulation of the soluble peptidoglycan precursor UDP-*N*-acetylmuramic acid-pentapeptide (UDP-MurNAc-pentapeptide) in the cytoplasm. Using membrane preparations and a complete cascade of purified, recombinant late stage peptidoglycan biosynthetic enzymes (MraY, MurG, FemX, PBP2) and their respective purified substrates, we showed that NAI-107 forms complexes with bactoprenol-pyrophosphate-coupled precursors of the bacterial cell wall. Titration experiments indicate that first a 1:1 stoichiometric complex occurs, which then transforms into a 2:1 (peptide: lipid II) complex, when excess peptide is added. Furthermore, lipid II and related molecules obviously could not serve as anchor molecules for the formation of defined and stable nisin-like pores, however, slow membrane depolarization was observed after NAI-107 treatment, which could contribute to killing of the bacterial cell.

Lanthipeptides are small (19–39 amino acids) ribosomally synthesized (1, 2) and post-translationally modified peptides, which are characterized by lanthionine and methyl-lanthionine containing intramolecular rings (3). The most prominent group of lanthipeptides are lantibiotics that are produced by and act on Gram-positive bacteria (4, 5). Lantibiotics are chemically and structurally very diverse; two subgroups of lantibiotics have been distinguished, based on differences in their structures and modes of action (6). Type A lantibiotics, such as nisin, are screw-shaped, elongated, flexible, and amphiphatic peptides with an overall positive net charge and pore-forming activities. Type B lantibiotics, *e.g.* mersacidin, are globular and carry either no net charge or are negatively charged. A more recent classification of lantibiotics in different subgroups has been proposed, based on the organization of their biosynthetic genes and enzymes, rather than on the activity profile or three-dimensional structure (3, 7). The activity of lantibiotics is based on different killing mechanisms, which may be combined in one molecule. The most extensively studied lantibiotic is nisin (8). It is produced by some *Lactococcus lactis* and widely used as a food preservative for more than 40 years. Like many lantibiotics nisin inhibits growth of Gram-positive bacterial strains by interfering with peptidoglycan through binding to the key intermediate lipid II (9–12).

Lipid II represents the central cell wall building block of peptidoglycan biosynthesis that is structurally conserved among eubacteria. The precursor consists of the bactoprenol carrier lipid (C_{55}-P), and is linked to the peptidoglycan building block *N*-acetylmuramyl-pentapeptide-*N*-acetylglucosamine (MurNAc-pp-GlcNAc) via a pyrophosphate bridge. Lipid II synthesis occurs at the inner face of the cytoplasmic membrane, where the translocase MraY and the transferase MurG link the soluble, UDP-activated sugars UDP-*N*-acetylmuramic acid-pentapeptide and UDP-*N*-acetylglucosamine to produce lipid I and lipid II, respectively. Lipid II is characteristically modified in different species. In staphylococci, the peptidyltransferases FemXAB catalyze the attachment of a pentaglycine-interpeptide bridge (13, 14) and the glutamate in position 2 of the stem-peptide is amidated to glutamine by the bienzyme complex MurT-GatD (15). The fully modified lipid II molecule is then

* This work was supported in part by grants from the European Commission within the LAPTOP-project (contract number 245066 for FP7-KBBE-2009-3) to the University of Bonn and NAICONS Srl and by the BONFOR program of the Medical Faculty of the University of Bonn.
[S] This article contains supplemental Tables S1 and S2 and Figs. S1 and S2.
[1] To whom correspondence may be addressed: Meckenheimer Allee 168, 53115 Bonn, Germany. Tel.: 49-0-28-735266; Fax: 49-0-228-735267; E-mail: dmuench@uni-bonn.de.
[2] Supported by a grant from the German federal state of North Rhine-Westphalia and the European Union (European Regional Development Fund "Investing in your future").
[3] To whom correspondence may be addressed. E-mail: hgsahl@uni-bonn.de.

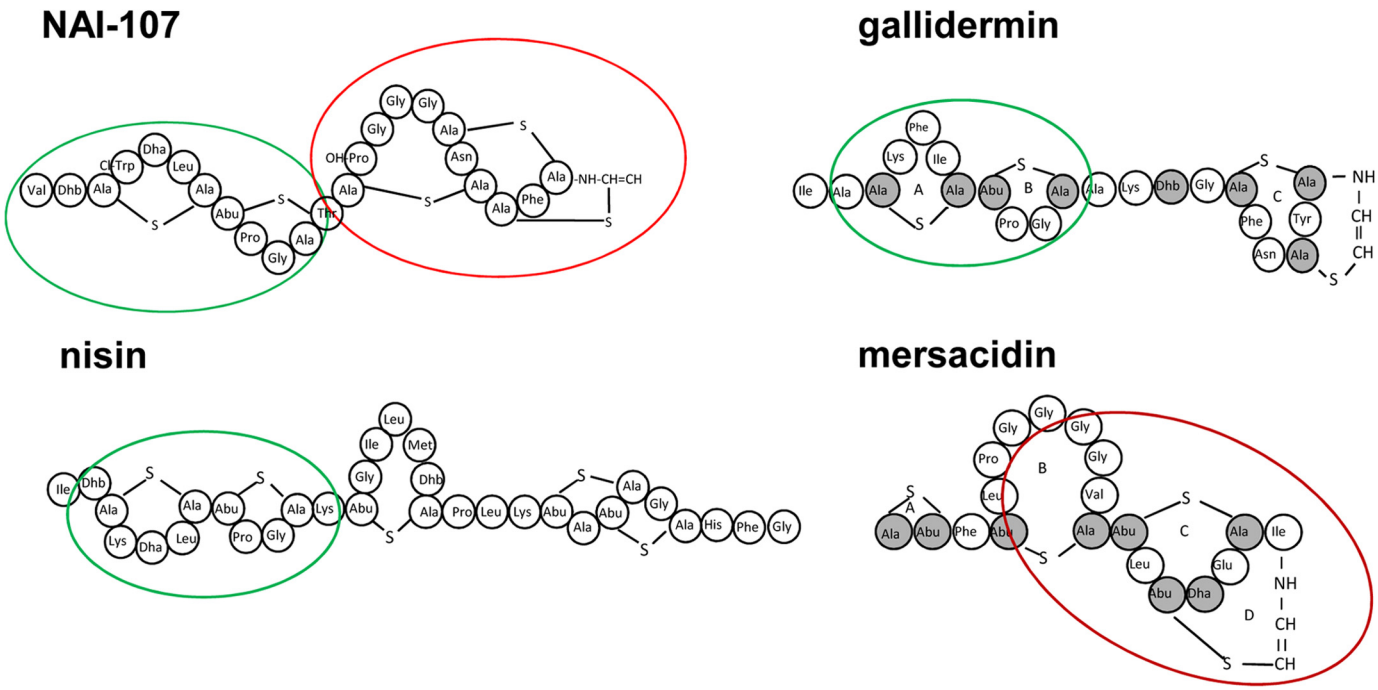

FIGURE 1. **Structures of the lantibiotics NAI-107, gallidermin, nisin, and mersacidin.** The nisin-like lipid II binding motif is highlighted in *green* and lipid II binding motifs similar to that found in mersacidin are marked *red* (22, 23).

translocated across the cytoplasmic membrane (16) where it is assembled into the growing peptidoglycan network through the activity of transglycosylases and transpeptidases (penicillin-binding protein (PBPs)), thereby releasing the C_{55}P-carrier, which after dephosphorylation enters a new synthesis cycle. Binding of nisin to lipid II locks the cell wall precursor in a stable complex, thereby blocking the entire peptidoglycan synthesis cycle. Additionally, nisin combines this activity with a unique target-mediated pore formation, using lipid II as a docking molecule, and causing dissipation of the membrane potential, rapid efflux of small metabolites, and cessation of cellular biosynthetic processes (17–19).

The renewed interest in the chemotherapeutic potential of antibacterial lantibiotics that inhibit cell wall synthesis originates from the fact that they are effective in treating infections sustained by methicillin-resistant *Staphylococcus aureus* and that they do not show cross-resistance with glycopeptides (7, 20). In fact, binding of lantibiotics does not involve the glycopeptide binding site, *i.e.* the C-terminal D-alanyl-D-alanine (D-Ala-D-Ala) moiety of the pentapeptide side chain. Rather, lantibiotics containing the nisin-like double ring system at the N terminus bind to the pyrophosphate linkage unit of lipid II, which equally blocks access of the transglycosylase to its substrate (21–23). For the same group of lantibiotics it has been recently shown that besides binding to lipid II, they interact with the lipid intermediates lipid III (undecaprenol-pyrophosphate-*N*-acetylglucosamine) and lipid IV (undecaprenol-pyrophosphate-*N*-acetylglucosamine-*N*-acetylmannosamine) of the wall teichoic acid (WTA)[4] biosynthesis pathway (24) all sharing the pyrophosphate moiety of the bactoprenol membrane anchor.

NAI-107 (Fig. 1), also known as microbisporicin or 107891 (20), is a new type AI lantibiotic produced by the actinomycete *Microbispora s.* ATCC PTA-5024, which is active against multidrug-resistant Gram-positive pathogens, including methicillin-resistant *S. aureus*, vancomycin-resistant *Enterococcus sp.*, penicillin-resistant *Streptococcus pneumoniae* and unusually for a lantibiotic, also against some Gram-negative species (20, 21). The compound was discovered during a screening program designed to detect all classes of cell-wall inhibitors except for β-lactams and glycopeptides (4). In addition to one methyllanthionine and three lanthionine bridges and a C-terminal S-((*Z*)-2-aminovinyl)-D-cysteine, modifications found in other lantibiotics, NAI-107 contains two unusually modified amino acids: 5-chlorotryptophan and 3,4-dihydroxyproline (16, 25). These modifications are unique to NAI-107 within the lantibiotic class of compounds and are rare in other ribosomally synthesized peptides. Genetic analysis previously identified the biosynthetic gene cluster and revealed insights into the pathway-specific regulation by an extracytoplasmic function σ-factor·anti-σ-factor complex (26, 27).

NAI-107 is produced as a complex of two major structurally related 24-amino acid variants (A1, 2246 Da; and A2, 2230 Da), which differ in proline 14 being monohydroxylated in variant A2, or bishydroxylated in variant A1 (28). Overall NAI-107 seems to combine two known lipid II targeting motifs (Fig. 1) with its 1–11 N-terminal sequence being similar to nisin and its C-terminal ring system, which shares structural elements with epidermin and mersacidin (3, 29). NAI-107 is currently in late preclinical development and displays efficacy in animal models of multidrug-resistant infections superior to the drugs of last resort, linezolid and vancomycin (30). Interestingly, NAI-107-

[4] The abbreviations used are: WTA, wall teichoic acid; MIC, minimal inhibitory concentration; DPC, dodecylphosphocholine; PRE, paramagnetic relaxation enhancement; PBP, penicillin-binding protein; BMA, 1,7-bis(methylcarbamoylmethyl)-1,4,7-triazaheptane-1,4,7-triacetic acid.

resistant mutants were not observed during these studies. Preliminary mode of action studies gave the first hints toward inhibition of cell wall biosynthesis (28). In the present study, we set out to identify the molecular target and the specific mechanism of action of the lantibiotic NAI-107.

MATERIALS AND METHODS

Susceptibility Testing—Determination of minimal inhibitory concentrations (MICs) was performed in 96-well polypropylene microtiter plates (Nunc) by standard broth microdilution in cation-adjusted Mueller-Hinton broth (Oxoid), according to the general guidelines provided by CLSI/NCCLS. NAI-107 was prepared essentially as described (31).

Killing Kinetics—*S. aureus* ATCC 29213 was grown overnight in half-concentrated Mueller Hinton Broth and diluted in fresh medium to an optical density (A_{600}) of 0.1. NAI-107 was added in concentrations corresponding to 1× and 2× MIC (4 and 8 μg/ml, respectively). Controls were made either without peptide or with the corresponding amount of dimethyl sulfoxide in the culture. The viable count was monitored up to 24 h. Aliquots were taken at defined intervals, especially focusing on the first 60 min. Colony counts were performed on serially diluted samples in 0.9% NaCl and 100 μl of the dilutions were plated onto MH agar plates. The plates were incubated at 37 °C and the colony forming units (cfu) were read after 24 h.

Incorporation of Radioactive Metabolites—The effect of NAI-107 on the synthesis of macromolecules was studied monitoring the incorporation of ^{3}H- or ^{14}C-labeled precursors (5-[^{3}H]thymidine, [^{3}H]glucosamine hydrochloride, and L-[^{14}C]isoleucine). An overnight culture of *Staphylococcus simulans* M22 grown in half-concentrated Mueller Hinton Broth containing 1 mM of the respective unlabeled metabolite was diluted 50-fold into fresh medium and cultured at 37 °C to an A_{600} of 0.5. Cultures were then split into two aliquots, diluted to an A_{600} of 0.04 and allowed to regrow to an A_{600} of 0.1. Subsequently, the respective labeled precursor was added to each culture (final concentration 1 μCi/ml); NAI-107 was added at 0.5× MIC or 1× MIC, and another aliquot was run as a control without adding peptide. Incorporation was monitored for up to 40 min. Macromolecules were precipitated with ice-cold TCA (10%) and incubated for at least 30 min on ice before being filtered through glass microfiber filters (Whatman). Filters were washed with 5 ml of TCA (2.5%) containing 10 mM unlabeled metabolite, dried, and counted.

Carboxyfluorescein Efflux from Lipid II Containing Liposomes—Large unilamellar vesicles were prepared by the extrusion technique, essentially as described by Wiedemann *et al.* (11). Vesicles were made of 1,2-dioleoyl-*sn*-glycerol-3-PC supplemented with 0.5 mol % of lipid II (referring to the total amount of phospholipid). Carboxyfluorescein-loaded vesicles were prepared with 50 mM carboxyfluorescein and then diluted in 1.5 ml of buffer (50 mM MES-KOH, 100 mM K_2SO_4, pH 6.0) at a final concentration of 25 μM phospholipid on a phosphorous base. After addition of the peptide, the increase of fluorescence intensity was measured at 520 nm (excitation at 492 nm) on an RF-5301 spectrophotometer (Shimadzu) at room temperature. Leakage was documented relative to the total amount of marker release after solubilization of the vesicles by addition of 10 μl of 20% Triton X-100.

Monitoring the Membrane Potential Using $DiBAC_4$—Cells of *Bacillus subtilis* 168, *S. aureus* ATCC 29213, and *Micrococcus luteus* DSM 1790 were grown in half-concentrated Mueller Hinton Broth to an A_{600} of 0.5 and incubated for 5 min with 1 μM of the membrane potential-sensitive fluorescent probe bis-(1,3-dibutylbarbituric acid)trimethine oxonol ($DiBAC_4$(3); Molecular Probes). NAI-107 was added at 10 times the MIC. 1 μM Nisin was used as positive control. Fluorescence was measured at the excitation and emission wavelengths of 492 and 515 nm, respectively.

Accumulation of N-Acetylmuramic Acid-Pentapeptide—*S. aureus* ATCC 29213 was grown in MH broth to an A_{600} of 0.7 and supplemented with 130 μg/ml of chloramphenicol. After 15 min antibiotics (NAI-107 or vancomycin) were added at 10× MIC and incubated for 30 min. Cells were harvested and extracted with boiling water. The suspension was then centrifuged (48,000 × *g*, 30 min) and the supernatant lyophilized. Nucleotide-linked cell wall precursors were analyzed by HPLC and corresponding fractions were confirmed by mass spectrometry.

Antagonization Assays—Antagonization of the antibiotic activity of NAI-107 by potential target molecules was performed by a MIC-based setup in microtiter plates. NAI-107 (20 μg/ml corresponding to 5× MIC) were mixed with potential HPLC-purified antagonists (UDP-MurNAc-pentapeptide, C_{55}-P, lipid I, lipid II) in a 10-fold molar excess with respect to the antibiotic. *S. aureus* ATCC 29213 (5×10^5 cfu/ml) was added and samples were examined for visible bacterial growth after overnight incubation.

Potassium Efflux from Whole Cells—For potassium efflux experiments a microprocessor pH meter (pH 213; Hanna Instruments, Kehl, Germany) with a MI-442 potassium electrode and MI-409F reference electrode was used. To obtain stable results, the electrodes were pre-conditioned by immersing both the potassium selective and the reference electrodes in choline buffer (300 mM choline chloride, 30 mM MES, 20 mM Tris, pH 6.5) for at least 1 h before starting calibration or measurements. Calibration was carried out before each determination by immersing the electrodes in fresh standard solutions containing 0.01, 0.1, or 1 mM KCl in choline buffer. Cells of *B. subtilis* 168 were grown in Mueller-Hinton Broth and harvested at an optical density (A_{600}) of 1.0 to 1.5 (3300 × *g*, 4 °C, 3 min), washed with 50 ml of cold choline buffer, and resuspended in the same buffer to an A_{600} of 30. The concentrated cell suspension was kept on ice and used within 30 min. For each measurement the cells were diluted in choline buffer (25 °C) to an A_{600} of about 3. Calculations of potassium efflux in percent were performed according to the equations established by Orlov *et al.* (32). Peptide-induced leakage was monitored for 3 min, with values taken every 10 s, and was expressed relative to the total amount of potassium release induced by addition of 1 μM nisin. NAI-107 was added at 10× MIC.

In Vitro Lipid I/Lipid II Synthesis and Purification—*In vitro* lipid II synthesis was performed using membranes of *M. luteus* as described (22, 33). In short, lipid I and lipid II were synthesized *in vitro* using membrane preparations of *M. luteus* DSM 1790. Membranes were isolated from lysozyme-treated cells by centrifugation (40,000 × *g*), washed twice in 50 mM Tris-HCl, 10 mM $MgCl_2$, pH 7.5, and stored under liquid nitrogen until use. Analytical assays were performed in a total volume of 150 μl containing 300–400 μg of membrane protein, 10 nmol of unde-

caprenylphosphate, 100 nmol of UDP-*N*-acetylmuramic acid pentapeptide (UDPMurNAc-pp), 100 nmol of UDP-GlcNAc in 60 mM Tris-HCl, 5 mM $MgCl_2$, pH 7.5, and 0.5% (w/v) Triton X-100. For purification of milligram quantities of lipid II, the analytical procedure was scaled up by a factor of 500. Reaction mixtures were incubated for 1 h at 28 °C, and lipids were extracted with the same volume of *n*-butanol, 6 M pyridine-acetate, pH 4.2. Lipid I was synthesized as described for lipid II with the omission of UDP-GlcNAc from the synthesis reaction. Purification of lipid I/lipid II was performed on a DEAE-FF column (5 ml; GE Healthcare) and eluted in a linear gradient from chloroform/methanol/water (2:3:1) to chloroform, methanol, 300 mM ammonium bicarbonate (2:3:1). Lipid I- and lipid II-containing fractions were identified by TLC (silica plates, 60F254; Merck) using chloroform/methanol/water/ammonia (88:48:10:1) as the solvent (13). Spots were visualized by phorbol 12-myristate 13-acetate staining reagent (34).

Analysis of Enzyme Activities—The overall lipid II synthesis reaction was performed as described above using membrane preparations of *M. luteus* DSM 1790 in a total volume of 150 μl. For quantitative analysis 0.5 nmol of [^{14}C]UDP-GlcNAc (7.4 GBq mmol^{-1}; Amersham Biosciences) was added to the reaction mixture. To determine the enzymatic activity of purified MraY-His_6 the assay was carried out in a total volume of 50 μl containing 5 nmol of C_{55}-P or [^{3}H]C_{55}-P (14.8 GBq/mmol; Biotrend), 50 nmol of UDP-MurNAc-pentapeptide in 100 mM Tris-HCl, 30 mM $MgCl_2$, pH 7.5, and 10 mM *N*-lauroylsarcosine. The reaction was initiated by the addition of 7.5 μg of the enzyme and incubated for 1 h at 37 °C. The MurG activity assay was performed in a final volume of 30 μl containing 2.5 nmol of purified lipid I, 25 nmol of UDP-GlcNAc or [^{14}C]UDP-GlcNAc in 200 mM Tris-HCl, 5.7 mM $MgCl_2$, pH 7.5, and 0.8% Triton X-100 in the presence of 0.45 μg of purified MurG-His_6 enzyme. The reaction mixture was incubated for 30 min at 30 °C. The assay for synthesis of lipid II-Gly_1 catalyzed by FemX was performed as described previously without any modifications (13). Enzymatic activity of PBP2 was determined by incubating 2.5 nmol of lipid II in 100 mM MES, 10 mM $MgCl_2$, pH 5.5, and 0.1% Triton X-100 in a total volume of 50 μl. The reaction was initiated by the addition of 7.5 μg of PBP2-His_6 and incubated for 1.5 h at 30 °C. The inhibitory effect on NAI-107 on WTA-precursor formation lipid III (undecaprenol-pyrophosphate-*N*-acetyl-glucosamine) and lipid IV (undecaprenyl-pyrophosphate-*N*-acetyl-glucosamine-*N*-acetylmannosamine) was investigated as described by Müller *et al.* (24). The enzymatic activity of the TagO-catalyzed lipid III synthesis was determined using purified recombinant TagO protein incubated in the presence of 5 nmol of C_{55}-P, 67.5 nmol of UDP-GlcNAc, and 0.75 nmol of [^{14}C]UDP-GlcNAc in 83 mM Tris-HCl, pH 8.0, 6.7 mM $MgCl_2$, 8.3% (v/v) dimethyl sulfoxide, and 10 mM *N*-lauroylsarcosine. The reaction was initiated by the addition of 6.15 μg of the enzyme TagO-His_6 and incubated for 90 min at 30 °C. TagA- and MnaA-catalyzed synthesis of lipid IV was performed using HPLC-purified lipid III. About 1 nmol of lipid III was incubated with 15 nmol of UDP-GlcNAc and 0.2 nmol of [^{14}C]UDP-GlcNAc in the presence of 0.2% Triton X-100, 100 mM Tris-HCl, pH 7.5, and 250 mM NaCl in a final volume of 50 μl. About 1.1 μg of TagA-His_6 and MnaA-His_6 was added to start the reaction. Synthesized lipid intermediates were extracted from the reaction mixtures with *n*-butanol/pyridine acetate, pH 4.2 (2:1; v/v), analyzed by thin layer chromatography (TLC) as described earlier (13). Radiolabeled spots were visualized by iodine vapor, excised from the silica plates and quantified by β-scintillation counting (1900 CA Tri-Carb scintillation counter; Packard). Analysis of the lipid II conversion catalyzed by PBP2 was carried out by applying reaction mixtures directly onto TLC plates developed in solvent B (butanol/acetic acid/water/pyridine (15:3:12:10, v/v/v/v)). Purification of WTA lipid intermediates was performed as described for lipid II with slight modifications (13). NAI-107 and nisin were added in various molar concentrations ranging from 0.5 to 2:1 with respect to the amount of purified C_{55}-P, lipid I, lipid II, lipid III, and lipid IV, respectively, in all *in vitro* assays.

Complex Formation of NAI-107 with Lipid II as Analyzed by TLC—Purified lipid II or ^{14}C-labeled lipid II (2 nmol) was incubated in 10 mM Tris-HCl, pH 7.5, in the presence of increasing NAI-107 concentrations (NAI-107:lipid II molar ratios ranging from 0.5 to 2:1) in a total volume of 30 μl. After incubation for 30 min at 25 °C, the mixture was analyzed by TLC using solvent B (butanol/acetic acid/water/pyridine; 15:3:12:10, v/v/v/v). Analysis was carried out by phorbol 12-myristate 13-acetate or ninhydrin staining or/and phosphoimaging (STORM Phosphorimager).

Microscopy—Sample preparation and bright field microscopy for examination of the cell shape after acetic acid/methanol fixation was performed as described by Schneider *et al.* (35) with minor modifications (36). Briefly, *B. subtilis* 168 was grown in Belitzky minimal medium and treated with antibiotics in early exponential growth phase. After 15 min of antibiotic stress cells were fixed in a 1:3 mixture of acetic acid and methanol, immobilized in low melting agarose, and microscopically examined.

Depolarization assays were performed with *B. subtilis* 1981 GFP-MinD (37) as reported recently (36). *B. subtilis* 1981 GFP-MinD was grown overnight in Belitzky minimal medium. Cells were then inoculated to an A_{500} of 0.1 in Belitzky minimal medium containing 0.1% xylose to induce expression of the GFP-MinD fusion protein. After reaching an A_{500} of 0.35, cells were exposed to 5 μg/ml of NAI-107. After 15 min of antibiotic stress, 0.5 μl of the bacterial culture was withdrawn and the nonfixed, nonimmobilized samples were imaged immediately in fluorescent mode. Pore formation was monitored in *B. subtilis* 168 using the live/dead BacLight bacterial viability kit (Invitrogen) as described previously (38). In short, exponentially growing cells were treated with antibiotics for 15 min. Subsequently, 2 ml of culture were incubated with 4 μl of a 1:1 mixture of the respective fluorescent dyes for another 15 min in the dark. Cells were washed and resuspended in TE buffer (100 mM Tris, 1 mM EDTA, pH 7.5). Five μl of the cell suspension were imaged without fixation or immobilization in fluorescent mode.

Proteome Analysis—MICs in Belitzky minimal medium were determined in test tubes under steady agitation. Growth inhibition experiments were performed to find an appropriate antibiotic concentration eliciting a sufficient proteome response. We selected a NAI-107 concentration that led to the up-regu-

lation of marker proteins without completely inhibiting biosynthesis of household proteins. Protein synthesis rates were determined by measuring the incorporation of radioactively labeled methionine into proteins prior to two-dimensional PAGE. Incorporation rates between 20,000 and 100,000 cpm/μg of crude protein were considered appropriate for proteome analysis (data not shown). Proteomic profiling of the acute bacterial stress response was performed with 0.9 μg/ml of NAI-107 (0.1× MIC). Radioactive labeling of newly synthesized proteins and subsequent separation of the cytosolic proteome by two-dimensional PAGE was performed as described previously (37). In short, 5 ml of a *B. subtilis* culture were exposed to antibiotics in early exponential growth phase. After 10 min cells were pulse-labeled with L-[^{35}S]methionine for 5 min. Radioactive incorporation was stopped by inhibition of protein biosynthesis by adding 1 mg/ml of chloramphenicol and an excess of non-radioactive methionine. Cells were harvested by centrifugation, washed three times with TE buffer, and disrupted by ultrasonication. Fifty-five μg of protein for analytical and 300 μg for preparative gels were loaded onto 24-cm immobilized pH 4–7 gradient strips (GE Healthcare) by passive rehydration for 18 h. Proteins were separated in a first dimension by isoelectric focusing and in a second dimension by SDS-PAGE using 12.5% acrylamide gels. Analytical gel images were analyzed as described previously (39, 40) using Decodon Delta 2D 4.1 image analysis software (Decodon, Greifswald, Germany). Proteins more than 2-fold up-regulated in three independent biological replicates were defined as marker proteins. Protein spots were identified either by MALDI-TOF measurements on a 4800 MALDI TOF/TOF Analyzer (Applied Biosystems, Foster City, CA) as described previously (PMID: 21383089) or by nanoUPLC-ESI-MS/MS as previously reported (38) using a Synapt G2S high definition mass spectrometer equipped with a lock spray source for electrospray ionization and a TOF detector (Waters, Milford, MA).

NMR Titration of Lipid II with NAI-107—A solution of lipid II in chloroform/methanol was dried under nitrogen and the residue was redissolved in a solution of 360 mM dodecylphosphocholine (DPC)-d_{38} (Cambridge Isotopes), 25 mM imidazole-d_4, 1 mM NaN_3, and 17.2 μM TSP-d_4 (sodium 2,2′,3,3′-tetradeutero 3-trimethylsilylpropionate) in 90% H_2O, 10% D_2O. The pH of the solution was measured to 6.50, the total volume was 0.55 ml. The lipid II content was quantified by integrating lipid II and TSP-d_4 NMR resonances to 2.65 mM.

^{1}H and ^{31}P NMR spectra were recorded, then NAI-107 was added as a dried aliquot and redissolved under vortexing. ^{1}H and ^{31}P NMR spectra were recorded for each titration point. Experiments were recorded on a BRUKER AVIII-600MHz spectrometer equipped with a BBFO+ RT-probe. All spectra were recorded at 310.1 K.

NAI-107 Structure in Micelle—3.5 mM NAI-107 was dissolved in 150 mM DPC-d_{38} in 5% D_2O at pH 6.2. A NOESY spectrum with 80 ms mixing time and two natural abundance ^{13}C-^{1}H-heteronuclear single quantum coherence spectra, one for the aliphatic signals, one for the aromatic signals, were recorded on a BRUKER AV-900MHz spectrometer equipped with a TCI cryoprobe. A TOCSY spectrum with 80 ms mixing time was recorded on a BRUKER DRX-600 MHz spectrometer equipped with a TCI cryoprobe. Both spectrometers belong to the Centre for Biomolecular Magnetic Resonance, Frankfurt, Germany. Insertion depth and orientation of NAI-107 in DPC micelles was determined as described in Ref. 41. Briefly, Inversion-Recovery weighted NOESY spectra were recorded in the absence of paramagnetic agent and in the presence of 1 and 2 mM Gd(DTPA-BMA). Relaxation rates of ^{1}H resonances were extracted and plotted *versus* the concentration of gadolinium. The slope of the line was taken as paramagnetic relaxation enhancement (PRE). The PREs were then converted to distance information as described in Ref. 41.

Structure Calculation—Integrated and assigned NOESY peak lists were used as input for the program CYANA (42) to calculate 20 structures. These 20 structures were further refined four times each in explicit solvent with YASARA (43) using the NOVA and YASARA force fields. For each of the four repetitions of a structures calculated, the one with the lowest residual violations was retained and thus, a final bundle of 20 structures was obtained.

TABLE 1
Antibacterial activity of NAI-107 against bacterial strains used in this study

Bacterial strain	MIC
	μg/ml
S. aureus ATCC 29213	4
S. simulans 22	4
B. subtilis 168	0.5
M. luteus DSM 1790	≤0.062

RESULTS

Antimicrobial Activity of NAI-107—NAI-107 exhibits potent antibacterial activity against a number of Gram-positive pathogens, including multiresistant strains such as methicillin-resistant *S. aureus*, penicillin-resistant *pneumococci*, and vancomycin-resistant *enterococci* (Table 1). Growth kinetic data of *S. aureus* ATCC 29213 exposed to NAI-107 resembled those obtained with cell wall-interfering agents (such as vancomycin, penicillin, and bacitracin), rather than rapidly lytic membrane-active agents such as polymyxin and novispirin (35). Consistently, killing kinetics indicated that over a period of approximately one generation time (0.5 h), treated cells were just unable to multiply before the number of colony-forming units decreased (data not shown).

Effect of NAI-107 on Whole Cells—NAI-107, at 0.5× MIC, inhibited the incorporation of radiolabeled glucosamine, an essential precursor of bacterial peptidoglycan, into cells of *S. simulans* M22 (Fig. 2*A*), whereas DNA, RNA, and protein biosynthesis were much less affected, suggesting cell wall biosynthesis as a potential target pathway. To distinguish whether NAI-107 interferes with the cytoplasmic or membrane-associated steps, we analyzed the cytoplasmic pool of UDP-linked peptidoglycan precursors in NAI-107-treated cells. Antibiotics that interfere with the late stages of peptidoglycan synthesis, such as vancomycin, are known to trigger accumulation of the ultimate soluble peptidoglycan precursor in the cytoplasm. Consistent with the results of the incorporation studies, NAI-107 treatment led to the intracellular accumulation of soluble precursor UDP-MurNAc-pentapeptide, however, to a lower

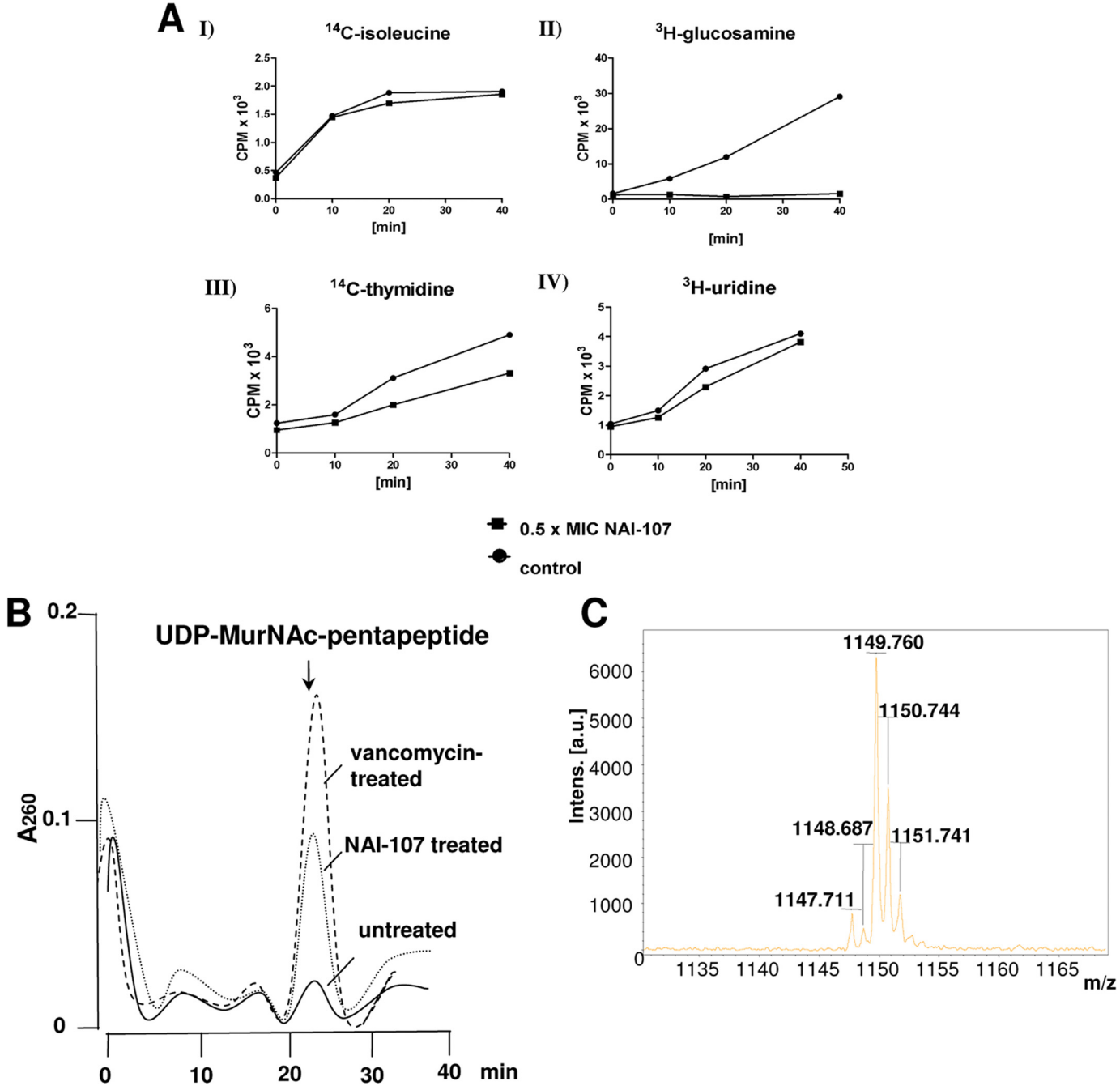

FIGURE 2. *A,* impact of NAI-107 on macromolecular biosyntheses of *S. simulans* M22. Untreated (*circles*) and NAI-107-treated (*squares*) cells were incubated with tritium-labeled precursors to monitor their incorporation into proteins (*I*), cell wall (*II*), DNA (*III*), and RNA (*IV*). *B,* intracellular accumulation of the soluble cell wall precursor UDP-MurNAc-pentapeptide in *S. aureus* ATCC 29213. Cells were treated with NAI-107 (*dotted line*) and vancomycin (*dashed line*), both at 10-fold MIC, or left untreated (*solid line*) for 60 min. Cells were harvested and extracted with boiling water. The suspension was then centrifuged and the supernatant lyophilized. *C,* UDP-MurNAc-pentapeptide was identified by means of mass spectrometry using the negative mode and 6-aza-2-thiothymine (in 50% (v/v) ethanol, 20 mM ammonium citrate) as matrix; the calculated monoisotopic mass is 1149.35.

extent, as compared with the vancomycin control (Fig. 2*B*), suggesting that the biosynthesis capacity of the cell was somewhat impaired, however, gross leakage of the precursor was not observed. This is in line with the fact that NAI-107 slightly affected the membrane potential of growing cells (Fig. 3*B*), suggesting an interaction with the membrane without formation of stable pores. Consistently, in contrast to the positive control nisin, no potassium leakage (Fig. 3*C*), nor carboxyfluorescein efflux from lipid II-containing liposomes was detected (Fig. 3*A*). Whole cell assays were repeated with different strains (*M. luteus* DSM 1790, *S. simulans*, *B. subtilis* 168, and *S. aureus* ATCC 29213) to exclude membrane effects dependent on membrane thickness and lipid composition of the target strain as described for gallidermin or epidermin (21, 29).

To better estimate the contribution of the slow membrane depolarization (Fig. 3*B*) and potassium leakage (Fig. 3*C*) to the overall killing activity, we applied fluorescent microscopy techniques and studied the impact of NAI-107 on localization of a

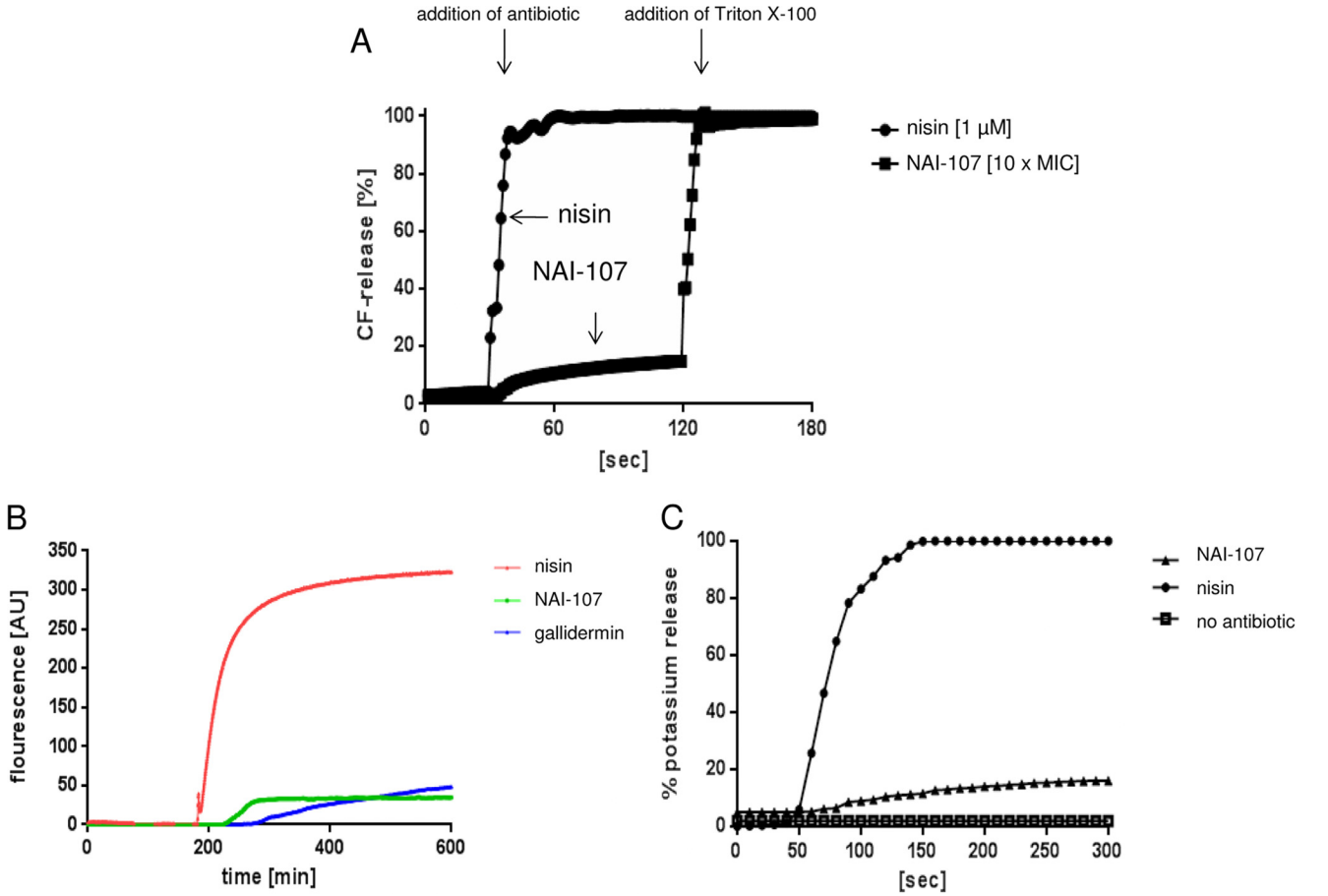

FIGURE 3. **Impact of NAI-107 on the integrity of bacterial and liposome membranes.** *A*, carboxyfluorescein efflux from lipid II containing liposomes. *B*, influence of NAI-107 on the membrane potential of *S. aureus* ATCC 29213 as analyzed using $DiBAC_4$. Antibiotics were added at concentrations corresponding to 10-fold MIC. Under these experimental conditions the δ-ψ of the untreated cells amounts to −140 mV, of nisin-depolarized cells to −60 mV (57) and of NAI-107 or gallidermin-treated cells to −120 to −110 mV, δ-ψ was determined using the ^{3}H-labeled tetraphenylphosphonium bromide ion as described (57). *C*, potassium efflux from *B. subtilis* 168 cells was monitored with a potassium-sensitive electrode. Ion leakage is expressed relative to the total amount of potassium released after addition of 1 μM pore-forming lantibiotic nisin (100%, *circles*). NAI-107 was added at 10× MIC (*triangles*); controls were without peptide antibiotics (*squares*).

GFP fusion to the cell division protein MinD. MinD is part of the cell division regulation machinery of *B. subtilis*. In energized cells, MinD is attached to the membrane and localizes at the cell poles and in the cell division plain, whereas in the presence of membrane-depolarizing agents like valinomycin or proton ionophore carbonyl cyanide *m*-chlorophenylhydrazone, MinD delocalizes appearing in irregular clusters (37). After treatment with NAI-107 for 15 min, such irregular dispersion of GFP-labeled MinD was observed (Fig. 4), demonstrating sufficient membrane depolarizing for MinD delocalization. A threshold potential, necessary for keeping MinD in place, has not been reported, however, it is likely that MinD delocalization after 15 min is in agreement with the level of depolarization observed after 5 min measured with $DIBAC_4$ (Fig. 3*B*). Using the green fluorescent dye SYTO 9 and the red fluorescing propidium iodide, we could also confirm that NAI-107 does not form stable pores or membrane holes. SYTO 9 diffuses through intact membranes, whereas propidium iodide can only enter bacterial cells through large pores or membrane holes. In a fluorescence overlay, perforated cells appear yellow, whereas intact cells appear green. Obviously NAI-107 did not efficiently facilitate penetration of propidium iodide into *B. subtilis* (Fig. 4), which is in line with our previous findings. Similar results were also reported for gallidermin and mersacidin (Table 2) (36).

Proteomic Response to NAI-107 Treatment—Depending on structural features, the level of interaction with the cytoplasmic membrane varies significantly among lipid II-targeting lantibiotics and range from mere binding to lipid II (mersacidin) to defined and stable pore formation (nisin) (10, 17, 23). In previous studies (36, 44–46) the impact of nisin, gallidermin, and mersacidin on cell wall integrity, pore formation, and membrane depolarization in *B. subtilis* was compared, and correlated to stress responses. Setting up a proteomic response reference library, including these lantibiotics, as well as other envelope-targeting antibiotics such as bacitracin, vancomycin, gramicidin S, or valinomycin, YtrE could be identified as the most reliable marker protein for interfering with membrane-bound steps of cell wall biosynthesis. Furthermore, NadE and PspA were identified as markers for antibiotics interacting primarily with the cytoplasmic membrane. In such an experiment NAI-107 treatment led to up-regulation of 20 protein spots compared with the untreated control, 15 of which could be identified by mass spectrometry (Fig. 5, supplemental Table S1). Among the

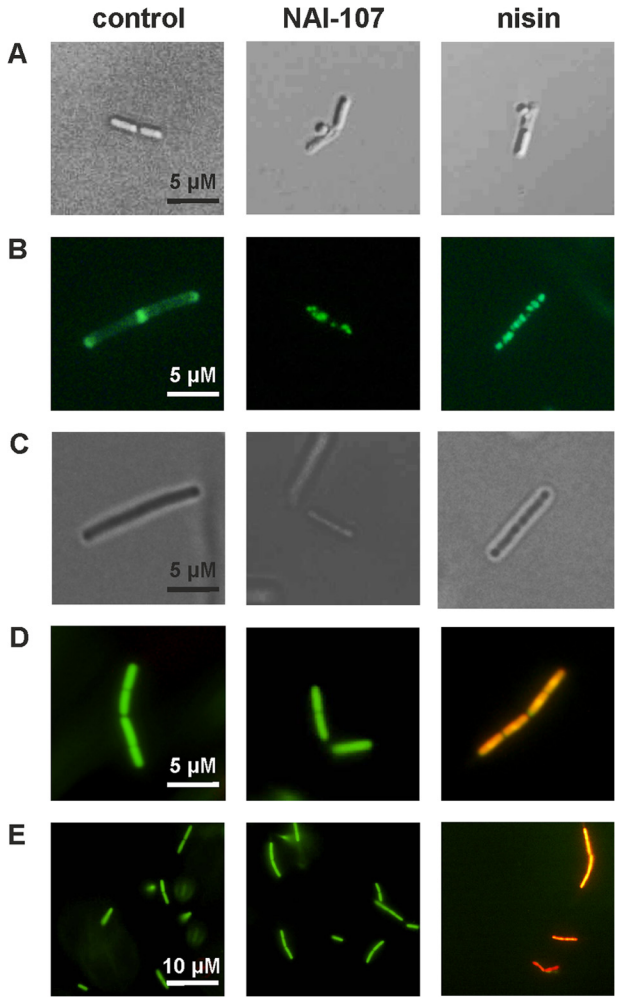

FIGURE 4. **Microscopy of *B. subtilis* cells treated with NAI-107 or nisin.** *A,* examination of the cell shape after acetic acid/methanol fixation. *B,* depolarization assays using *B. subtilis* 1981 GFP-MinD. *C,* light microscopy of cells in *B. D* and *E,* membrane depolarization as monitored with the live/dead BacLight bacterial viability kit: (*D*) individual cells and (*E*) overview. Images of control and nisin-treated cells in *D* were taken from Ref. 58.

identified proteins were LiaH, YtrB, YtrE, and YpuA (formerly referred to as NGM1 (35)), which are specific markers for inhibition of membrane-bound steps of cell wall biosynthesis and typically up-regulated by antibiotics interfering with lipid II or undecaprenylphosphate (36). LiaH is also up-regulated in response to compounds interfering with membrane architecture and localization of peripheral membrane proteins like MurG. Furthermore, YceC and YceH, which had been defined as cell envelope stress markers, and PspA and NadE, were found to be up-regulated in NAI-107-treated cells. Hence, NAI-107 elicits a typical dual cell wall biosynthesis and membrane stress response. The response strongly overlaps with that of gallidermin-treated cells, suggesting high mechanistic similarity between these two lantibiotics. Gallidermin integrates into membranes, with pore formation occurring only in some bacteria and correlating with membrane thickness and fatty acid branching (29, 36, 47). In contrast to nisin, which needs to dock to lipid II for membrane integration and pore formation, gallidermin shows very high association and low dissociation constants for binding to phospholipid bilayers, indicating that it readily integrates into the membrane independently of lipid II binding. Similarity of the proteome response profile of NAI-107 was also observed with MP196 and gramicidin S, both of which also integrate into the cytoplasmic membrane and disturb membrane architecture (36). Less overlap was observed with the response to nisin, which is dominated by rapid pore formation and membrane depolarization.

Impact of NAI-107 on in Vitro Peptidoglycan Biosynthesis—Membrane preparations of *M. luteus* have sufficient enzyme activity (MraY, MurG) for the formation of cell wall precursors lipid I and lipid II *in vitro*. Testing the overall lipid II synthesis reactions with such membranes, to which defined amounts of C_{55}-P, as well as the soluble precursors UDP-MurNAc-pentapeptide and UDP-GlcNAc, were added, we found that NAI-107 blocked the formation of lipid II as observed by TLC (Fig. 6*A*). In the positive control, where no inhibitor was present, the complete conversion of C_{55}-P to lipid II was achieved. Quantitative analysis using [^{14}C]UDP-GlcNAc to specifically label lipid II revealed a concentration-dependent reduction of the lipid II amount. Addition of equimolar concentrations of NAI-107 with respect to C_{55}-P resulted in a 69% decrease in extractable lipid II, and a 2-fold molar excess of the lantibiotic completely blocked lipid II synthesis (Fig. 6*B*).

For detailed analysis, we focused on the individual cell-wall biosynthesis steps *in vitro* using purified recombinant enzymes from *S. aureus* (MurG, FemX, PBP2) in the presence of NAI-107. For these enzymes, lipid I (MurG) or lipid II (FemX, PBP2) are substrates, and significant inhibition of the reactions was observed when NAI-107 was added in 2-fold molar excess with respect to lipid I or lipid II (Fig. 6*B*), strongly suggesting that NAI-107 may form a stoichiometric complex with the substrates rather than inhibiting the enzymes.

To confirm that the activity of NAI-107 is primarily based on the formation of a complex with lipid I/lipid II, we performed conventional MIC determinations in the presence of C_{55}-P, lipid I, lipid II, UDP-GlcNAc, and UDP-MurNAc-pentapeptide at 5-fold molar concentrations with respect to the concentration of NAI-107. The activity of NAI-107 was only antagonized in the presence of lipid I and lipid II (data not shown), which agrees well with its inhibition of the MurG-, FemX-, and PBP2-catalyzed reactions, in which lipid I and lipid II are substrates. Binding of NAI-107 and lipid II was further validated by incubating purified lipid II together with NAI-107 in various molar concentrations ranging from 0.5 to 2 in respect to the lipid precursor. Subsequent TLC was used to analyze the migration behavior (Fig. 7). Free lipid II migrated to a defined position (Fig. 7, *A* and *B, first lane*), whereas free NAI-107 was only detectable by ninhydrin staining (Fig. 7*A, second lane*). However, in complex with NAI-107, lipid II remained at the start point, appearing as a ring-like structure (Fig. 7, *A, third lane*, and *B, second* to *fourth lanes*). As has been observed in the cell-free assays, only at a 2:1 ratio, no free lipid II was detectable, substantiating the formation of a 2:1 stoichiometric NAI-107·lipid II complex in our *in vitro* test system.

Interaction of NAI-107 with WTA Precursors—Binding of nisin and related lantibiotics to lipid II mainly involves the pyrophosphate and the MurNAc moiety (23), whereas the second sugar (GlcNAc) does not appear to significantly contribute.

TABLE 2
Table of protein spots identified in two-dimensional gel and their corresponding functions

Protein ID	Protein function	Functional category
CysC	Adenylyl-sulfate kinase	Sulfur metabolism
GamA	Glucosamine-6-phosphate deaminase	Cell wall
LiaH	Similar to phage shock protein	Cell wall
LiaR	Two-component response regulator, regulation of the *liaI-liaH-liaG-liaF-liaS-liaR* operon	Cell wall
NadE	NAD synthase	Energy
NrfA	Spx-dependent FMN-containing NADPH-linked nitro/flavin reductase	Energy
PbpC	Penicillin-binding protein	Cell wall
PspA	Phage shock protein	Membrane
RpsB	Ribosomal protein	Translation
YceC	Similar to tellurium resistance protein	Cell envelope
YceH	Similar to toxic anion resistance protein	Cell envelope
YpuA	Unknown	Cell envelope
YqiG	Similar to NADH-dependent flavin oxidoreductase	Energy
YtrE	ABC transporter (ATP-binding protein)	Transport
YvcR	ABC transporter (ATP-binding protein) for the export of lipid II-binding lantibiotics	Transport
YvIB	Unknown	Cell envelope

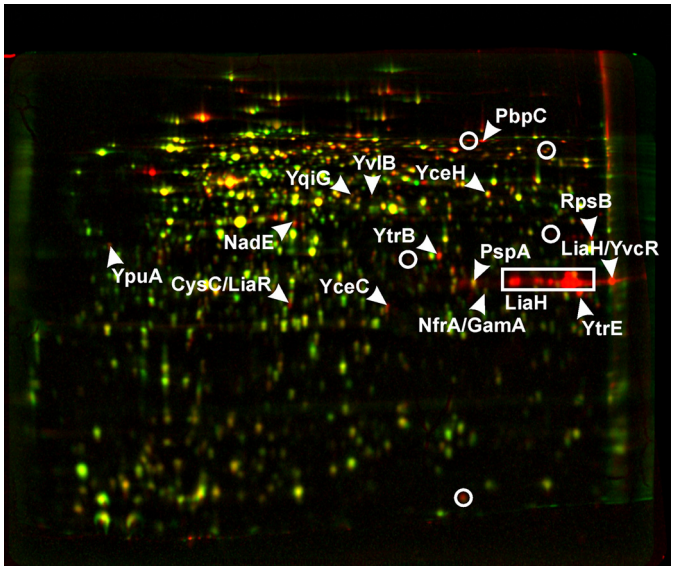

FIGURE 5. **Differential proteome analysis of *B. subtilis* 168 in response to NAI-107.** Two-dimensional gel-based protein synthesis profiles of the controls false colored in *green* were overlaid with those of the antibiotic-treated samples false colored in *red*. In the overlays, down-regulated proteins appear *green*, up-regulated proteins appear *red*, and proteins expressed at equal rates appear *yellow*.

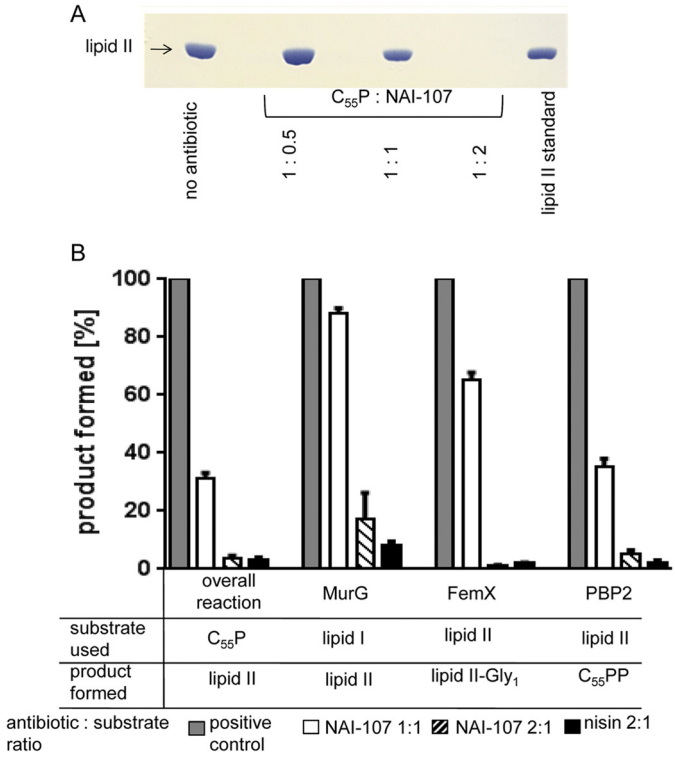

FIGURE 6. **Effect of NAI-107 on membrane-associated stages of peptidoglycan synthesis *in vitro*.** *A*, *in vitro* lipid II synthesis catalyzed by *M. luteus* membrane preparations. Thin layer chromatography of *n*-butanol/pyridine acetate extracts and detection by phosphomolybdic acid staining. NAI-107 was added to the reaction mixtures at molar ratios in respect to C_{55}P as indicated. 2 nmol of purified lipid II was run as a standard. *B*, synthesis and analysis of the individual biosynthesis steps were performed as described under "Materials and Methods." Bactoprenol containing products were analyzed by TLC. Product containing bands were visualized by iodine vapor, excised, and counted. Radiolabeling was based on ^{3}H-labeled C_{55}P (for lipid I), [^{14}C]GlcNAc for lipid II, and [^{14}C]glycine for lipid II-Gly$_1$. For all reactions, the amount of products synthesized by control reactions in the absence of antibiotic was set to 100%. NAI-107 was added at molar ratios of 1:1 and 2:1 with respect to the lipid substrates as indicated. The lantibiotic nisin in a 2-fold molar excess served as a control. Mean values from three independent experiments are shown. *Error bars* indicate the standard deviation.

Because lipid III and lipid IV, the first lipid intermediates of the WTA biosynthesis pathway (48, 49), have similar pyrophosphate sugar linkage moieties, we investigated the impact of NAI-107 on these reactions using recombinantly purified enzymes TagO, TagA, and MnaA (24). Only about 35% of the product ^{14}C-lipid III could be detected when NAI-107 was added at a 2-fold molar excess with respect to C_{55}-P, suggesting that NAI-107 forms a stable complex with lipid III, which escapes extraction of the lipid intermediate from the synthesis mixture, as described also for the nisin·lipid III complex (24). Quantitative analysis of the TagA-catalyzed lipid IV synthesis reaction using radiolabeled UDP-GlcNAc also revealed dose-dependent inhibition by NAI-107 and nisin (Fig. 8). Added in equimolar concentrations, NAI-107 inhibited the formation of lipid IV, compared with a positive control, where no antibiotic was added, to about 45%. At a molar ratio of 2:1 (NAI-107:lipid), NAI-107 inhibited the synthesis of radiolabeled lipid IV to about 80%.

NMR Studies—To gain further insight into the nature of the NAI-107/lipid II interaction at the membrane interface, we attempted to follow the process by NMR spectroscopy (Fig. 9). At first, lipid II was titrated with NAI-107. To keep aggregate sizes as low as possible, we utilized micelles of DPC as membrane models (supplemental Fig. S1). The ^{31}P NMR resonances

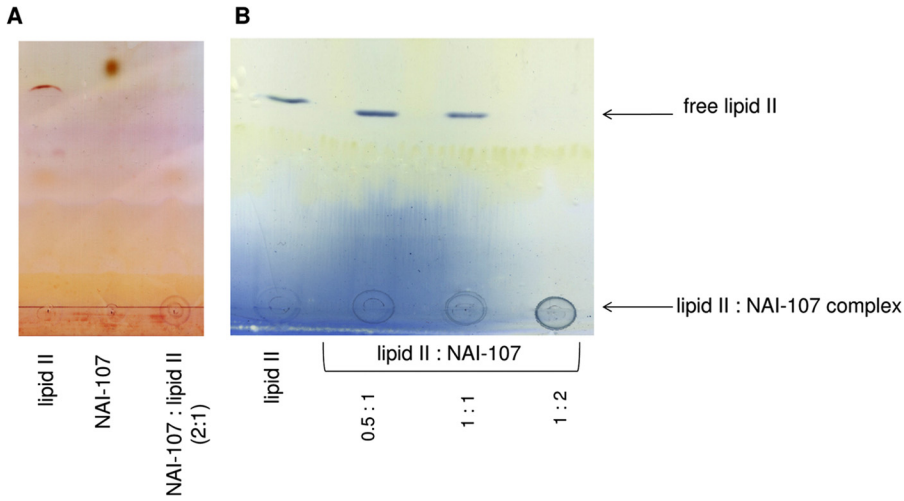

FIGURE 7. **Complex formation of NAI-107 with lipid II and estimation of binding stoichiometry.** Lipid II was incubated with NAI-107 at the indicated molar ratios. The stable complex of NAI-107 with lipid II remains close to the application spot, whereas free lipids and NAI-107 migrate to the indicated positions. *A,* ninhydrin staining. *First lane,* free lipid II (2 nmol); *second lane,* NAI-107 (4 nmol); *third lane,* NAI-107:lipd II molar ratio 2:1. *B,* phorbol 12-myristate 13-acetate staining of lipid II incubated with increasing molar ratios of NAI-107. Free NAI-107 could not be detected with phorbol 12-myristate 13-acetate staining. Spots were separated using Solvent B (see "Materials and Methods").

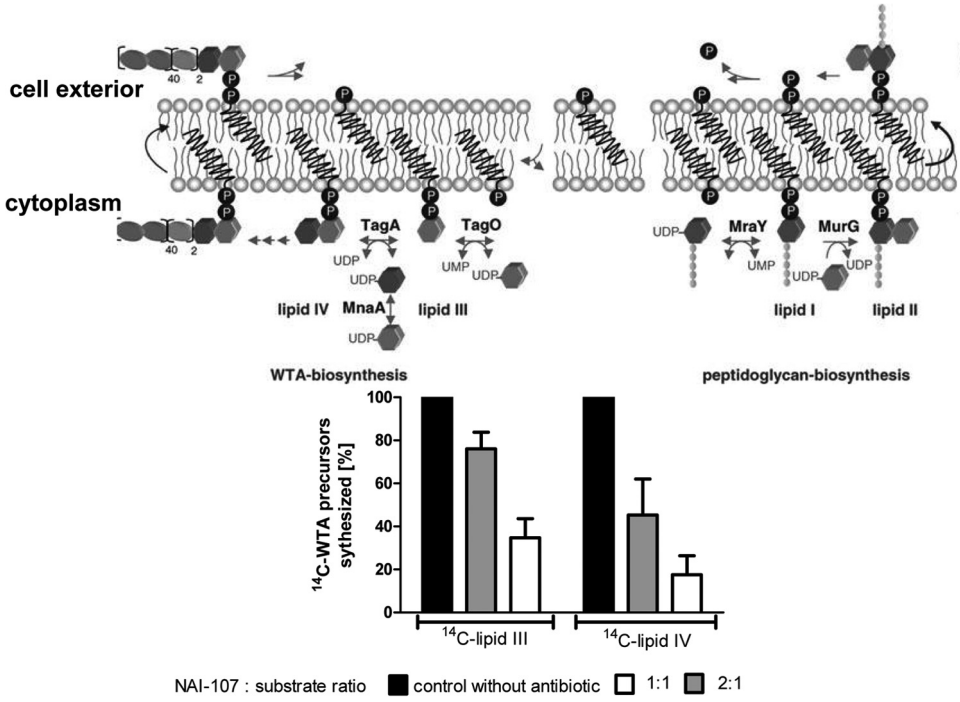

FIGURE 8. *Top,* schematic representation of peptidoglycan and WTA biosynthesis. *Bottom*, impact of NAI-107 on the lipid III and lipid IV synthesis. For lipid III synthesis purified recombinant TagO protein was incubated in the presence of 5 nmol of C_{55}-P and [^{14}C]UDP-GlcNAc. The reaction was initiated by the addition of 6.15 μg of the enzyme TagO-His_6 and incubated for 90 min at 30 °C. For lipid IV synthesis, TagA was incubated with purified lipid III and [^{14}C]UDP-GlcNAc. The reaction was initiated by the addition of 1.1 μg of MnaA and TagA and incubated for 4 h at 30 °C. NAI-107 was added at molar ratios of 1 and 2 with respect to the substrate C_{55}P or lipid III. Reaction products were extracted with BuOH/PyrAc (2:1) and separated by TLC. Detection and quantification were carried out using a Storm Phosphorimager.

of lipid II were followed through the titration (supplemental Fig. S2*A*). In the course of the titration, signals of free lipid II disappear up to a molar ratio of 1:1, however, no signals of any bound form seem to appear. At a molar ratio of 1:1, only NMR signals of buffer components are seen. Further addition of NAI-107 leads to the reappearance of ^{31}P NMR signals. The same is seen when looking at ^{1}H NMR spectra throughout the titration (supplemental Fig. S2*B*). When going from 0:1 (NAI-107:lipid II) to 1:1, lipid II signals gradually disappear. No new signals appear, nor are there visible signals of NAI-107. Visible signals appeared only at molar ratios for NAI-107:lipid II >1:1. Integration of ^{31}P spectra can be used to follow the amounts of different species throughout the titration. The resonance at −16.3 ppm was integrated, assumed to stem from one phosphorous atom of free lipid II, the region from −17.0 to −19.0 was integrated, assumed to stem from two phosphorous atoms of bound lipid II in a NAI-107·lipid II 2:1 complex. The ^{31}P resonance of DPC was used as an internal standard for integra-

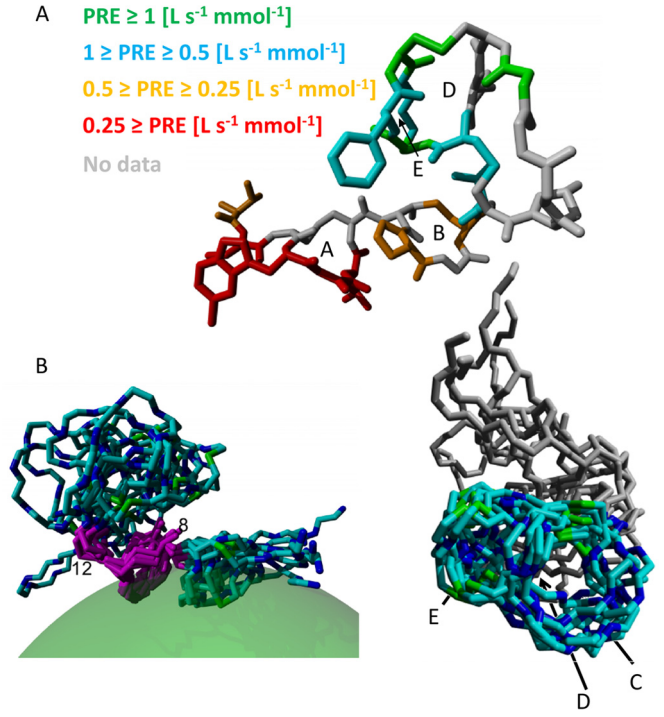

FIGURE 9. *A*, structure of NAI-107 in DPC micelles (conformer with lowest energy of constraint violation) with residues colored according to PRE. Letters *A–E* indicate the lanthionine rings. For better visibility, the whole residue was colored even though an experimental PRE was obtained only for one or two hydrogen atoms fixed to the backbone. Lower PRE values indicate less contact with the solvent/larger distance to the solvent, *i.e.* deeper penetration into the micelle. As a rule of thumb, residues with PRE ≈ 0.5 (liters s^{-1} $mmol^{-1}$) are located at the micelle-water interface, residues in *orange* are located in the polar part of the micelle, residues in *red* are buried in the hydrophobic part of the micelle, whereas residues with higher PREs (*cyan* and *green*) are located outside the micelle. *B*, structure of NAI-107 in DPC micelles. The bundle of 10 structure with lowest root mean square deviation, superimposed on residues 8–12 is shown with the DPC micelle of the first structure indicated as semi-transparent *green sphere*. *Right panel*, bundle of 10 structures with the lowest root mean square deviation superimposed on residues 12–24, letters *C*, *D*, and *E* indicate lanthionine rings.

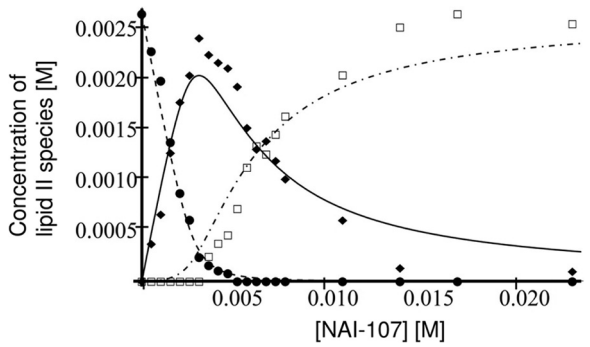

FIGURE 10. **Titration of 2.65 mM lipid II with NAI-107: concentration of free lipid II (●), concentration of NAI-107·lipid II 1:1 complex (♦), concentration of NAI-107·lipid II 2:1 complex (□).** The theoretical concentrations, assuming sequential binding with $K_{a1} = 2 \times 10^4$ (M^{-1}) and $K_{a2} = 450$ (M^{-1}) are shown as a *dashed line* for free lipid II, *full line* for the 1:1 complex, and *dot-dashed line* for the 2:1 complex.

tion between spectra. The integral of the first sample of pure lipid II was assumed to be 100% free lipid II and used to calculate free lipid II concentrations at all titration points. The integral of the last titration sample was assumed to be 100% NAI-107·lipid II 2:1 complex and was used to calculate NAI-107·lipid II 2:1 complex concentrations at all titration points. The NAI-107·lipid II 1:1 complex does not yield any quantifiable NMR signals, thus its concentration was back-calculated by subtracting the concentrations of free and 2:1 complex from the total concentration of lipid II in the sample. The concentrations of the three different species of lipid II during the course of titration are shown in Fig. 10.

Subsequently, we studied the interaction of NAI-107 with membrane mimetic, DPC micelles. NAI-107, which is insoluble in pure water, readily dissolves in water in the presence of 150 mM DPC. The appearance of ^{1}H NMR spectra also suggests that the correlation time of NAI-107 in the presence of micelles is higher than that of NAI-107 dissolved in 30% acetonitrile, indicating substantial interaction with the micelle.

Chemical shifts of NAI-107 were assigned in the presence of DPC micelles and NOEs were collected. In addition, paramagnetic relaxation enhancement of NAI-107 backbone atoms by Gd(DTPA-BMA) in the bulk solution were determined and converted to distances from the micellar center. These data together were then used to simultaneously calculate the structure of NAI-107 in DPC micelles and its insertion into the micelle. Fig. 9*A* illustrates the distribution of paramagnetic relaxation enhancements throughout the structure. Fig. 9*B* shows the structure of NAI-107 bound to the micelle. Statistical data on the structure can be found in supplemental Table S2. As can be expected for short peptides, the structure is quite dynamic, resulting in elevated root mean square deviation values. NMR assignments and molecular coordinates have been deposited at the BMRB (accession number 19619) and PDB databases (Protein Data Bank code 2mh5), respectively.

DISCUSSION

The increasing level of antibiotic resistance is a threat to human health, and existing classes of antibiotics need to be further developed or entirely new classes need to be identified. For the most challenging groups of multiresistant Gram-positive bacteria, the lipid II-binding antibiotics offer excellent possibilities for development. Generally, targets such as the sugar-pyrophosphate moiety in lipid II, which is recognized by many lantibiotics (23), cannot be altered as easily as protein targets, or more variable sugar moieties, and the D-Ala-D-Ala terminus of lipid II. Detailed mode-of-action studies of lantibiotics, such as NAI-107, demonstrate the multiplicity of activities that can be achieved when high affinity binding of lipid II is combined with direct effects on the cytoplasmic membrane, be it defined pore formation like with nisin or insertion and subsequent impact on membrane functionality, like with NAI-107. The integration of NAI-107 into the membrane certainly affects protein localization and promotes disorganization of the highly dynamic biosynthesis and energy generating protein machineries. Such membrane activities are intrinsic features of cationic amphiphilic compounds and are also characteristic for some of the glyco(lipo)peptides and glycodepsipeptides like telavancin, dalbavancin, and oritavancin (50, 51) that are on the market or in late-stage clinical investigations. Notably, the increase in amphiphilicity, at least in some cases, not only enhances antibiotic potency and bactericidal activity, but also impacts positively on pharmacokinetic parameters and enables favorable once daily or even once weekly dosage schemes.

NAI-107 interacts with cell envelope precursors attached to the undecaprenylphosphate (C_{55}-P) carrier molecule, such as lipid I and lipid II and those for WTA biosynthesis (Fig. 8). In this context, the accessibility of WTA precursors must be taken into account to evaluate their importance as targets *in vivo*. As lipid III and lipid IV are further processed to the linear WTA polymer on the cytoplasmic side, they could only function as targets after internalization of the lantibiotic. Nisin translocation across lipid bilayers, which may occur in the course of pore formation, has been observed in several studies (9, 52–54). Whether this is true for NAI-107 remains to be determined. The fully assembled C_{55}P-linked WTA polymer, exported to the outside, seems to be the most likely candidate for a relevant target, as it is the only WTA building block exposed at the cellular surface (Fig. 8). Although NAI-107 has the highest affinity for lipid II, which we consider its primary target, it is possible that, if supplied at high concentrations, the antibiotic will recognize the other targets as well, simultaneously trapping the bactoprenol carrier at several sites and causing general depletion of the undecaprenyl pool. Interaction with multiple targets is beneficial in light of reduced resistance development, and therefore an advantage of NAI-107. In general, bacterial cells, which are exposed to antibiotic binding to the lipid II pyrophosphate linkage, do not merely suffer from inhibition of the transglycosylation step in peptidoglycan synthesis. Such lantibiotics appear to have a profound impact on the correct localization of lipid II (55) and presumably disrupt the functional organization of cell envelope biosynthesis machineries that rely on the C_{55}P carrier.

The 2:1 binding stoichiometry observed in most assay systems raised the question whether NAI-107 forms dimers in solution, or whether one peptide binds to lipid II followed by recruitment of another molecule of NAI-107. The latter mechanism is known from some two-peptide lantibiotics, such as lacticin 3147, where significant antibiotic activity is only achieved through the cooperative action of two peptides. Peptide A contains a mersacidin-like lipid II binding motif and binds to the CW precursor; the second peptide is then able to dock to the peptide·lipid II complex, allowing the complex to insert into the membrane to form a defined pore (56). We did not find evidence for a dimerization in solution, but the data showed clear evidence for two separate events in NAI-107·lipid II binding, a relatively strong initial interaction leading to the disappearance of free lipid II resonances and a weaker subsequent interaction leading to the appearance of bound lipid II and NAI-107 resonances (supplemental Fig. S2). It is puzzling that we do not observe any resonances of the complex at 1:1 stoichiometry. This could be explained by either conformational exchange at a time scale comparable with NMR chemical shift differences ($\approx 10^{-3}$–10^{-2} s^{-1}) or by the formation of larger aggregates.

^{31}P NMR shows a change in chemical shifts of lipid II phosphorous resonances upon interaction with NAI-107. The two atoms change their shift by approximately −2 and −4 ppm. This is similar to the changes observed upon binding of nisin to lipid II (23). Therefore, it is reasonable to assume that also NAI-107 binds to the pyrophosphate moiety. Because the pyrophosphate moiety can be expected to locate at the interface between the solution and the cellular membrane, it makes sense to look for the binding site of NAI-107 to lipid II around this interface. NMR data clearly show that NAI-107 interacts with the membrane mimetic at rings A and, to a lesser extent, B. The pyrophosphate group carries a negative charge, and the only positive charge in the whole NAI-107 molecule is located at the N terminus preceding ring A, and also this charge is located at the interface between bulk water and membrane mimetic. Taken together, the data point at an N-terminal interaction site of NAI-107 with lipid II, as is also the case for nisin. The sequence similarity between nisin and NAI-107 around rings A and B (Fig. 1) supports this interpretation, however, nisin has one more positive charge in ring A (Lys-4) compared with NAI-107, which has the unusual 5-chloro-Trp at this position.

Acknowledgments—We thank Dirk Albrecht (University of Greifswald, Germany) for MALDI-TOF analysis. We thank the Centre for Biomolecular Magnetic Resonance, Frankfurt, Germany, for access to NMR equipment and Dr. Frank Löhr for expert assistance. Michaele Josten provided excellent technical help. The NMR laboratory at Aalborg University is supported by the Obel, SparNord, and Carlsberg Foundations as well as part of the Danish Center for Antibiotic Research and Development (DanCARD) financed by Danish Council for Strategic Research Grant 09-067075. The Synapt G2S mass spectrometer was supported by the state of North Rhine Westphalia (Forschungsgroßgeräte der Länder).

REFERENCES

1. Arnison, P. G., *et al.* (2013) Ribosomally synthesized and post-translationally modified peptide natural products: overview and recommendations for a universal nomenclature. *Nat. Prod. Rep.* **30,** 108–160
2. Schnell, N., Entian, K.-D., Schneider, U., Götz, F., Zähner, H., Kellner, R., and Jung, G. (1988) Prepetide sequence of epidermin a ribosomally synthesized antibiotic with four sulphide rings. *Nature* **333,** 276–278
3. Chatterjee, C., Paul, M., Xie, L., and van der Donk, W. A. (2005) Biosynthesis and mode of action of lantibiotics. *Chem. Rev.* **105,** 633–684
4. Jabes, D., and Donadio, S. (2010) Strategies for the isolation and characterization of antibacterial lantibiotics. *Methods Mol. Biol.* **618,** 31–45
5. Willey, J. M., and van der Donk, W. A. (2007) Lantibiotics: peptides of diverse structure and function. *Annu. Rev. Microbiol.* **61,** 477–501
6. Sahl, H. G., and Bierbaum, G. (1998) Lantibiotics: Biosynthesis and biological activities of uniquely modified peptides from gram-positive bacteria. *Annu. Rev. Microbiol.* **52,** 41–79
7. Cotter, P. D., Hill, C., and Ross, R. P. (2005) Bacterial lantibiotics: strategies to improve therapeutic potential. *Curr. Protein Pept. Sci.* **6,** 61–75
8. Rogers, L. (1928) The inhibiting effect of *Streptococcus lactis* on *Lactobacillus bulgaricus*. *J. Bacteriol.* **16,** 321–325
9. Breukink, E., Wiedemann, I., van Kraaij, C., Kuipers, O. P., Sahl, H. G., and de Kruijff, B. (1999) Use of the cell wall precursor lipid II by a pore-forming peptide antibiotic. *Science* **286,** 2361–2364
10. Brötz, H., Josten, M., Wiedemann, I., Schneider, U., Götz, F., Bierbaum, G., and Sahl, H. G. (1998) Role of lipid-bound peptidoglycan precursors in the formation of pores by nisin, epidermin and other lantibiotics. *Mol. Microbiol.* **30,** 317–327
11. Wiedemann, I., Breukink, E., van Kraaij, C., Kuipers, O. P., Bierbaum, G., de Kruijff, B., and Sahl, H. G. (2001) Specific binding of nisin to the peptidoglycan precursor lipid II combines pore formation and inhibition of cell wall biosynthesis for potent antibiotic activity. *J. Biol. Chem.* **276,** 1772–1779
12. Breukink, E., and de Kruijff, B. (2006) Lipid II as a target for antibiotics. *Nat. Rev. Drug Discov.* **5,** 321–332
13. Schneider, T., Senn, M. M., Berger-Bächi, B., Tossi, A., Sahl H. G., and Wiedemann, I. (2004) *In vitro* assembly of a complete, pentaglycine inter-

peptide bridge containing cell wall precursor (lipid II-Gly_5) of *Staphylococcus aureus*. *Mol. Microbiol.* **53,** 675–685
14. Rohrer, S., and Berger-Bächi, B. (2003) FemABX peptidyl transferases: a link between branched-chain cell wall peptide formation and β-lactam resistance in Gram-positive cocci. *Antimicrob. Agents Chemother.* **47,** 837–846
15. Münch, D., Roemer, T., Lee, S. H., Engeser, M., Sahl, H. G., and Schneider, T. (2012) Identification and *in vitro* analysis of the GatD/MurT enzyme-complex catalyzing lipid II amidation in *Staphylococcus aureus*. *Plos Pathog.* **8,** e1002509
16. Van Heijenoort, Y., Derrien, M., and Van Heijenoort, J. (1978) Polymerization by transglycosylation in the biosynthesis of the peptidoglycan of *Escherichia coli* K12 and its inhibition by antibiotics. *FEBS Lett.* **89,** 141–144
17. Ruhr, E., and Sahl, H. G. (1985) Mode of action of the peptide antibiotic nisin and influence on the membrane potential of whole cells and on cytoplasmic and artificial membrane vesicles. *Antimicrob. Agents Chemother.* **27,** 841–845
18. Sahl, H. G., and Brandis, H. (1982) Mode of action of the staphylococcin-like peptide Pep 5 and culture conditions affecting its activity. *Zentralbl Bakteriol Mikrobiol Hyg A* **252,** 166–175
19. Sahl, H. G., Kordel, M., and Benz, R. (1987) Voltage-dependent depolarization of bacterial membranes and artificial lipid bilayers by the peptide antibiotic nisin. *Arch. Microbiol.* **149,** 120–124
20. Castiglione, F., Lazzarini, A., Carrano, L., Corti, E., Ciciliato, I., Gastaldo, L., Candiani, P., Losi, D., Marinelli, F., Selva, E., and Parenti, F. (2008) Determining the structure and mode of action of microbisporicin, a potent lantibiotic active against multiresistant pathogens. *Chem. Biol.* **15,** 22–31
21. Brötz, H., Bierbaum, G., Reynolds, P. E., and Sahl, H. G. (1997) The lantibiotic mersacidin inhibits peptidoglycan biosynthesis at the level of transglycosylation. *Eur. J. Biochem.* **246,** 193–199
22. Brötz, H., Bierbaum, G., Leopold, K., Reynolds, P. E., and Sahl, H. G. (1998) The lantibiotic mersacidin inhibits peptidoglycan synthesis by targeting lipid II. *Antimicrob. Agents Chemother.* **42,** 154–160
23. Hsu, S. T., Breukink, E., Tischenko, E., Lutters, M. A., de Kruijff, B., Kaptein, R., Bonvin, A. M., and van Nuland, N. A. (2004) The nisin–lipid II complex reveals a pyrophosphate cage that provides a blueprint for novel antibiotics. *Nat. Struct. Mol. Biol.* **11,** 963–967
24. Müller A., Ulm, H., Reder-Christ, K., Sahl, H. G., and Schneider, T. (2012) Interaction of type A lantibiotics with undecaprenol bound cell envelope precursors. *Microb. Drug Resist.* **18,** 261–270
25. Lazzarini, A., Gastaldo, L., Cadiani, G., Ciciliato, I., Losi, D., Marinelli, F., Selva, E., and Parenti, F. (April 1, 2008) US Patent US7351687 B2 Antibiotic 107891, its factors A1 and A2, pharmaceutically acceptable salts and compositions, and use thereof
26. Foulston, L. C., and Bibb, M. J. (2010) Microbisporicin gene cluster reveals unusual features of lantibiotic biosynthesis in actinomycetes. *Proc. Natl. Acad. Sci. U.S.A.* **107,** 13461–13466
27. Foulston, L., and Bibb, M. (2011) Feed-forward regulation of microbisporicin biosynthesis in *Microbispora corallina*. *J. Bacteriol.* **193,** 3064–3071
28. Jabés, D., Brunati, C., Candiani, G., Riva, S., Romanó, G., Donadio, S. (2011) Efficacy of the new lantibiotic NAI-107 in experimental infections induced by multidrug-resistant Gram-positive pathogens. *Antimicrob. Agents Chemother.* **55,** 1671–1676
29. Bonelli, R. R., Schneider, T., Sahl, H. G., Wiedemann, I. (2006) Insights into *in vivo* activities of lantibiotics from gallidermin and epidermin mode-of-action studies. *Antimicrob. Agents Chemother.* **50,** 1449–1457
30. Castiglione, F., Cavaletti, L., Losi, D., Lazzarini, A., Carrano, L., Feroggio, M., Ciciliato, I., Corti, E., Candiani, G., Marinelli, F., and Selva, E. (2007) A novel lantibiotic acting on bacterial cell wall synthesis produced by the uncommon actinomycete *Planomonospora* sp. *Biochemistry* **46,** 5884–5895
31. Vasile, F., Potenza, D., Marsiglia, B., Maffioli, S., and Donadio, S. (2012) Solution structure by nuclear magnetic resonance of the two lantibiotics 97518 and NAI-107. *J. Pept. Sci.* **18,** 129–134
32. Orlov, D. S., Nguyen, T., and Lehrer, R. I. (2002) Potassium release, a useful tool for studying antimicrobial peptides. *J. Microbiol. Methods* **49,** 325–328
33. Umbreit, J. N., and Strominger, J. L. (1972) Isolation of the lipid intermediate in peptidoglycan biosynthesis from *Escherichia coli*. *J. Bacteriol.* **112,** 1306–1309
34. Rick, P. D., Hubbard, G. L., Kitaoka, M., Nagaki, H., Kinoshita, T., Dowd, S., Simplaceanu, V., and Ho, C. (1998) Characterization of the lipid-carrier involved in the synthesis of enterobacterial common antigen (ECA) and identification of a novel phosphoglyceride in a mutant of *Salmonella typhimurium* defective in ECA synthesis. *Glycobiology* **8,** 557–567
35. Schneider, T., Kruse, T., Wimmer, R., Wiedemann, I., Sass, V., Pag, U., Jansen, A., Nielsen, A. K., Mygind, P. H., Raventós, D. S., Neve, S., Ravn, B., Bonvin, A. M., De Maria, L., Andersen, A. S., Gammelgaard, L. K., Sahl, H. G., and Kristensen, H. H. (2010) Plectasin, a fungal defensin, targets the bacterial cell wall precursor lipid II. *Science* **328,** 1168–1172
36. Wenzel, M., Kohl, B., Münch, D., Raatschen, N., Albada, H. B., Hamoen, L., Metzler-Nolte, N., Sahl, H. G., and Bandow, J. E. (2012) Proteomic response of *Bacillus subtilis* to lantibiotics reflects differences in interaction with the cytoplasmic membrane. *Antimicrob. Agents Chemother.* **56,** 5749–5757
37. Strahl, H., and Hamoen, L. W. (2010) Membrane potential is important for bacterial cell division. *Proc. Natl. Acad. Sci. U.S.A.* **107,** 12281–12286
38. Wenzel, M., Patra, M., Senges, C. H. R., Ott, I., Stepanek, J. J., Pinto, A., Prochnow, P., Vuong, C., Langklotz, S., Metzler-Nolte, N., and Bandow, J. E. (2014) Analysis of the mechanism of action of potent antibacterial hetero-tri-organometallic compounds: a structurally new class of antibiotics. *ACS Chem. Biol.* **8,** 1442–1450
39. Wenzel, M., Patra, M., Albrecht, D., Chen, D. Y., Nicolaou, K. C., Metzler-Nolte, N., and Bandow, J. E. (2011) Proteomic signature of fatty acid biosynthesis inhibition available for in vivo mechanism-of-action studies. *Antimicrob. Agents Chemother.* **55,** 2590–2596
40. Bandow, J. E., Baker, J. D., Berth, M., Painter, C., Sepulveda, O. J., Clark, K. A., Kilty, I., and VanBogelen, R. A. (2008) Improved image analysis workflow for 2D gels enables large-scale 2D gel-based proteomics studies: COPD biomarker discovery study. *Proteomics* **8,** 3030–3041
41. Franzmann, M., Otzen, D., and Wimmer, R. (2009) Quantitative use of paramagnetic relaxation enhancements for determining orientations and insertion iepths of peptides in micelles. *ChemBioChem* **10,** 2339–2347
42. Güntert, P., Mumenthaler, C., and Wüthrich, K. (1997) Torsion angle dynamics for NMR structure calculation with the new program DYANA. *J. Mol. Biol.* **273,** 283–298
43. Krieger, E., Koraimann, G., and Vriend, G. (2002) Increasing the precision of comparative models with YASARA NOVA: a self-parameterizing force field. *Proteins* **47,** 393–402
44. Bandow, J. E., Brötz, H., Leichert, L. I., Labischinski H., and Hecker, M. (2003) Proteomic approaches to antibiotic drug discovery. *Antimicrob. Agents Chemother.* **47,** 948–955
45. Wenzel, M., and Bandow, J. E. (2011) Proteomic signatures in antibiotic research. *Proteomics* **11,** 3256–3268
46. Brötz-Oesterhelt, H., Beyer, D., Kroll, H. P., Endermann, R., Ladel, C., Schroeder, W., Hinzen, B., Raddatz, S., Paulsen, H., Henninger, K., Bandow, J. E., Sahl, H. G., and Labischinski, H. (2005) Dysregulation of bacterial proteolytic machinery by a new class of antibiotics. *Nat. Med.* **11,** 1082–1087
47. Christ, K., Al-Kaddah, S., Wiedemann, I., Rattay, B., Sahl, H. G., and Bendas, G. (2008) Membrane lipids determine the antibiotic activity of the lantibiotic gallidermin. *J. Membr. Biol.* **226,** 9–16
48. Brown, S., Zhang, Y. H., and Walker, S. (2008) A revised pathway proposed for *Staphylococcus aureus* wall teichoic acid biosynthesis based on *in vitro* reconstitution of the intracellular steps. *Chem. Biol.* **15,** 12–21
49. Xia, G., Kohler, T., and Peschel, A. (2010) The wall teichoic acid and lipoteichoic acid polymers of *Staphylococcus aureus*. *Int. J. Med. Microbiol.* **300,** 148–154
50. Barrett, J. F. (2005) Recent developments in glycopeptide antibacterials. *Curr. Opin. Investig. Drugs.* **6,** 781–790
51. Kim, S. J., Cegelski, L., Stueber, D., Singh, M., Dietrich, E., Tanaka, K. S., Parr, T. R., Jr., Far, A. R., and Schaefer, J. (2008) Oritavancin exhibits dual mode of action to inhibit cell-wall biosynthesis in *Staphylococcus aureus*. *J. Mol. Biol.* **377,** 281–293
52. Wiedemann, I., Benz, R., and Sahl, H. G. (2004) Lipid II-mediated pore

formation by the peptide antibiotic nisin: a black lipid membrane study. *J. Bacteriol.* **186,** 3259–3261
53. Breukink, E., Ganz, P., de Kruijff, B., and Seelig, J. (2000) Binding of nisin Z to bilayer vesicles as determined with isothermal titration calorimetry. *Biochemistry* **39,** 10247–10254
54. Scherer, K., Wiedemann, I., Ciobanasu, C., Sahl, H. G., and Kubitscheck, U. (2013) Aggregates of nisin with various bactoprenol-containing cell wall precursors differ in size and membrane permeation capacity. *Biochim. Biophys. Acta* **1828,** 2628–2636
55. Hasper, H. E., Kramer, N. E., Smith, J. L., Hillman, J. D., Zachariah, C., Kuipers, O. P., de Kruijff, B., and Breukink, E. (2006) Alternative bactericidal mechanism of action for lantibiotic peptides that target lipid II. *Science* **313,** 1636–1637
56. Wiedemann, I., Böttiger, T., Bonelli, R. R., Wiese, A., Hagge, S. O., Gutsmann, T., Seydel, U., Deegan, L., Hill, C., Ross, P., and Sahl, H. G. (2006) The mode of action of the lantibiotic lacticin 3147: a complex mechanism involving specific interaction of two peptides and the cell wall precursor lipid II. *Mol. Microbiol.* **61,** 285–296
57. Schneider, T., Gries, K., Josten, M., Wiedemann, I., Pelzer, S., Labischinski, H., and Sahl, H. G. (2009) The lipopeptide antibiotic friulimicin B inhibits cell wall biosynthesis through complex formation with bactoprenol phosphate. *Antimicrob. Agents Chemother.* **53,** 1610–1618
58. Wenzel, M., Chiriac, A. I., Otto, A., Zweytick, D., May, C., Schumacher, C., Gust, R., Albada, H. B., Penkova, M., Kramer, U., Erdmann, R., Metzler-Nolte, N., Straus, S. K., Bremer, E., Becher, D., Brotz-Oesterhelt, H., Sahl, H. G., Brandow, J. E. (2014) Small cationic antimicrobial peptides delocalize peripheral membrane proteins. *Proc Natl. Acad. Sci. U.S.A.*, in press, 10.1073/pnas.131199001